Applications in Energy and Combustion Science 26 (2026) 100510

Contents lists available at ScienceDirect

Applications in Energy and Combustion Science

journal homepage: www.sciencedirect.com/journal/applications-in-energy-and-combustion-science

Spotting ignition of pine needle bed by multiple hot steel particles

Supan Wang [a], Wenhao Xu [a], Chunyin Zhang [a], Xinyan Huang [b,*], Carlos Fernandez-Pello [c]

[a] College of Safety Science and Engineering, Nanjing Tech University, Nanjing, China
[b] Department of Building Environment and Energy Engineering, The Hong Kong Polytechnic University, Kowloon, Hong Kong
[c] Department of Mechanical Engineering, University of California Berkeley, USA

ARTICLE INFO

Keywords:
Wildfires
WUI fires
Spotting ignition limit
Smoldering-to-flaming transition
Wind speed
Particle distribution

ABSTRACT

Ignition of natural fuels by numerous small hot metal particles is an important pathway for wildfire initiation associated with power lines and mechanical operations. This work explores the ignition of a pine needle bed by hundreds of 2-mm diameter stainless steel hot particles deposited as a particle spray over an initial landing area, with fuel moisture content (MC) of up to 45% and wind speed up to 8 m/s. Increasing the particle number or mass facilitates direct flaming ignition, whereas the smoldering-to-flaming (StF) transition significantly lowers the ignition threshold in terms of particle area densities, defined as the ratio of total particle mass to the initial particle scattering area, with a minimum particle area density found at 0.4 g/cm^2 for 5% MC. A localized dispersion of particles ignites the fuel more effectively than distributed ones due to reduced environmental cooling and stronger inter-particle heating. Fires initiated by multiple particles also exhibit more extensive and faster fire spread than those from a single particle of equivalent energy. The ignition via StF transition is promoted by higher wind speed and lower fuel MC, where opposed smoldering spread exceeds concurrent spread under a small wind (~ 0.5 m/s). The ignition delay of smoldering and StF transition depends on the location and extent of the reaction zone, while being insensitive to the total mass and distribution of particles. Finally, a simplified heat transfer analysis links the spotting ignition threshold and delay time under different moisture and wind conditions based on a minimum char-layer thickness.

1. Introduction

The Wildland-Urban Interface (WUI) fires are recently becoming more frequent worldwide and have demonstrated the complex nature of this globally important problem [1–6]. Wildland fires are often initiated by small spot ignition sources, which may originate either from natural firebrands (i.e., burning vegetative fragments lofted by an existing fire) or from hot metal particles generated by human activities such as fireworks discharge, metal welding or grinding operations, or transmission line faults [5–7]. Firebrands are typically lightweight combustible embers capable of long-distance transport, whereas hot metal particles are non-combustible but thermally intense fragments that can directly heat fuels upon contact. Once a spotting fire is initiated, a fast fire spread with more firebrand generation is possible driven by ambient winds and fire plumes toward larger unburned areas [8]. Post-disaster investigations of major wildfires, such as 1987 Black Dragon fire [9], US 2018 Camp Fire [10], and 2019–2020 Australian bushfire season [11], have demonstrated that both firebrand-driven spotting and ignition by hot metal particles is critical to predict the propagation of wildland fires and fire emergency response, especially in the wildland-urban interface (WUI). Past research has predominantly focused on the critical particle size and initial temperature of various fuels using either large firebrands (piles) or a single/few large hot metal particles. In contrast, research on the ignition behavior of a larger number of tiny hot metal particles remains limited.

Research on the ignition of firebrands or firebrand shower has been conducted in literature. Manzello et al. [12–14] conducted full-scale experiments of burning vegetation and building components to character the production rates, size and mass distribution of firebrands. By analyzing controlling factors of firebrand generation, they identified the influence of vegetation type, moisture content, and fire intensity on firebrand production characteristics [15]. Past research on ignition induced by firebrands is mainly conducted to study whether a single firebrand particle, multiple firebrand particles, or firebrand shower can ignite a fuel bed after landing on it. These studies have quantified the hot-particle ignition limits (e.g., critical particle temperature, size, and energy) for various fuel beds, from fine wildland fuels (like pine needles, leaf litter, mulch, and peat soil) [16–19] to large structural components

* Corresponding author.
E-mail address: xy.huang@polyu.edu.hk (X. Huang).

https://doi.org/10.1016/j.jaecs.2026.100510
Received 7 January 2026; Received in revised form 3 April 2026; Accepted 1 May 2026
Available online 1 May 2026

(like wood roofs, decking, and facade) [7,19–22]. Lin et al. [18] deposited self-extinguishing, glowing cylindrical wooden firebrands (0.64 cm × 2.54 cm, varying masses) ignited by a propane burner onto different ground cover surfaces to quantify the critical conditions for smoldering ignition and subsequent smoldering-to-flaming (StF) transition. The combined effects of a hot particle or firebrand showers and radiant heat from other nearby combustibles are also investigated recently [24–26], and present the importance of continuous arrival of firebrands for fuel bed ignition. Therefore, it is reasonable to fundamentally study how bulk small-particle behavior affects hot-particle ignition.

Particle sizes generated from cutting processes have typically been reported in the submillimeter to 1 mm range [27], while welding processes can produce particles up to 5 mm in size [28]. A fundamental understanding on the spotting ignition of wildland fuels by a single hot particle has been extensively studied. Stokes et al. [29,30] investigated the influence of particle metal material on igniting combustible, discovering that steel and aluminum particles exhibit a higher ignition propensity than copper particle. Urban et al. [31] conducted ignition tests on grass mixture powders by a single hot particle of varying temperatures and materials to indicate a hyperbolic relationship between critical ignition temperatures and particle diameter for direct flaming and smoldering ignition. Furthermore, smoldering ignition was observed to require lower critical ignition conditions than flaming ignition [32–34]. The subsequent studies further compared the ignition capability of high-temperature aluminum particles on materials such as paper strips, hay, and pine needles [35–37]. They also found powered fuels could be ignited at lower temperatures, which verified that the morphology of the combustible material influences its susceptibility to ignition.

Our previous work [17] revealed that the hot metal particle acts as both heating and pilot sources like a small flame for direct flaming ignition of pine needle bed, but only acts as a heating source for smoldering ignition. Later, the single-particle ignition propensity, subsequent flame-spread and burning process of three WUI fuels (straw, pine needles, and cotton) were also determined [38]. Nevertheless, there is a notable lack of research on the ignition behavior of small multi-particles, such as those generated in fireworks discharge, power grid faults, metal welding, grinding and many other mechanical operations.

The moisture content (MC) of forest fuels, typically defined on a dry-weight basis, is one of the key parameters determining wildfire risk and often exhibits a wide range of variation. For example, under drought conditions, the MC of pine needles may be as low as 4%. However, within one hour following a weather change (e.g., precipitation), the MC of dead pine needles can increase to 40%, while that of live pine needles can even exceed 200% [39]. Fire spread over wet pine-needle beds under different MCs and wind speeds was investigate in [40], which revealed complex interactions between smoldering and flaming. Weather plays a key role in fire behavior by determining fuel moisture content, which in turn negatively affects parameters such as fire spread rate, combustion rate, and flame height [41]. Our previous work [17] quantified the effects of moisture and wind on the hot-particle ignition limit and ignition delay time by a single hot steel spherical particle. Wind was found to have a significant impact on the smoldering ignition of moist pine needles by affecting the glowing combustion state of the firebrand [42]. However, existing studies addressing the effects of wind speed and moisture have largely focused on single-particle ignition, whereas research involving multiple hot particles, typical of welding or grinding operations, remains limited.

This work investigates the spotting ignition by multiple hot metal particle (2-mm steel balls) on pine needle fuel beds with varying MCs and ambient wind conditions. Various multi-particle ignition phenomena and the interaction between flaming and smoldering are studied and analyzed in detail. Ignition limits were experimentally quantified correlating with both the particle number, total mass, and the scatter area. Additionally, ignition delay time was measured and analyzed to characterize the influencing factors of total particle mass, fuel moisture content, and wind speed.

2. Experimental methods

2.1. Multiple particles and fuel bed

The release of multiple particles was tested to mimic hot-particle ignition in practical scenarios such as welding, fireworks, or cutting processes. Different quantities of 2-mm-diameter 304 stainless steel hot particles (Fig. 1(a)), with a density of 7,687 ± 7 kg/m^3 and a specific heat capacity of 500 J/(kg·K), were selected based on energy equivalence. The 2-mm diameter particles were selected because it fell within the size range reported for welding processes in the literature [28] and allowed a controlled equivalent-energy comparison between multiple-particle and single-particle ignition. For instance, 125 particles of 2 mm diameter are approximately energy-equivalent to one 10-mm particle. Stainless steel was selected because of its engineering relevance, extensive use in previous hot-particle ignition studies, and good thermal stability at elevated temperatures. The ignition characteristics of particles with other materials will be investigated in future work.

Table 1 presents the mass-particle count relationship for 2-mm-diameter stainless steel particles, based on measured particle mass, experimentally measured scattering area, and calculated equivalent diameter and spotting particle mass area. Because the deposited particle cluster was not densely packed, gaps and irregular shapes naturally occurred within the scattering area shown in Fig. 1a. To account for these features in a simplified manner, the average particle area density was defined as the total mass divided by the average initial scattering area.

The fresh pine needles (Pinus massoniana) were collected from Sichuan (south-west China in a humid subtropical climate), with lengths of 12–22 cm and diameters of 0.5 ± 0.2 mm. The freshly collected needles were first air-dried at room temperature for over 15 days to obtain dead pine needles with a moisture content (MC) of 13 ± 2%. These air-dried samples were then oven-dried at 80°C for 3 h to obtain the driest fuel condition, with an MC of 5 ± 1%. The wetter samples (15 ± 1%, 25 ± 1%, 35 ± 2%, and 45 ± 2%), simulating seasonal and weather-induced fluctuations in forest fuel moisture, were prepared by spraying different amounts of distilled water onto the oven-dried samples, followed by sealing in airtight bags for at least 48 h to allow moisture equilibration. Before the ignition experiments, the MC of the samples was measured at different locations using an infrared moisture meter (MA160-1CN) to confirm moisture uniformity.

The prepared fuel beds, with a dry bulk density of 40 ± 5 kg/m^3, were uniformly distributed in 250 × 250 × 50 mm^3 metal mesh frames placed on an insulated fire-resistant base. To ensure uniformity and comparability across tests, the pine needles were intentionally aligned in a single direction following established practice [17], thereby creating a more isotropic fuel bed and minimizing the influence of fuel-bed orientation on ignition. This methodology aligns with established protocols for characterizing fuel properties.

2.2. Experimental procedure

The experimental setup of multi-hot particle ignition is illustrated in Fig. 1. It was constructed to observe the effects of particle spray, i.e., the release and deposition of multiple hot particles onto the fuel bed, on the ignition of a representative forest fuel bed. Different quantities of 2 mm diameter stainless steel hot particles were heated using a premixed-flame burner torch, as shown in Fig. 1(a). After 5 minutes of heating, the local representative temperature of the heated particle bed was verified using a calibrated K-type thermocouple inserted into the heated particles, giving a nominal value of approximately 980 ± 20°C prior to particle release. Because the current setup does not allow precise temperature control or direct measurement of the surface temperature of each individual particle temperature, this study focuses on the ignition

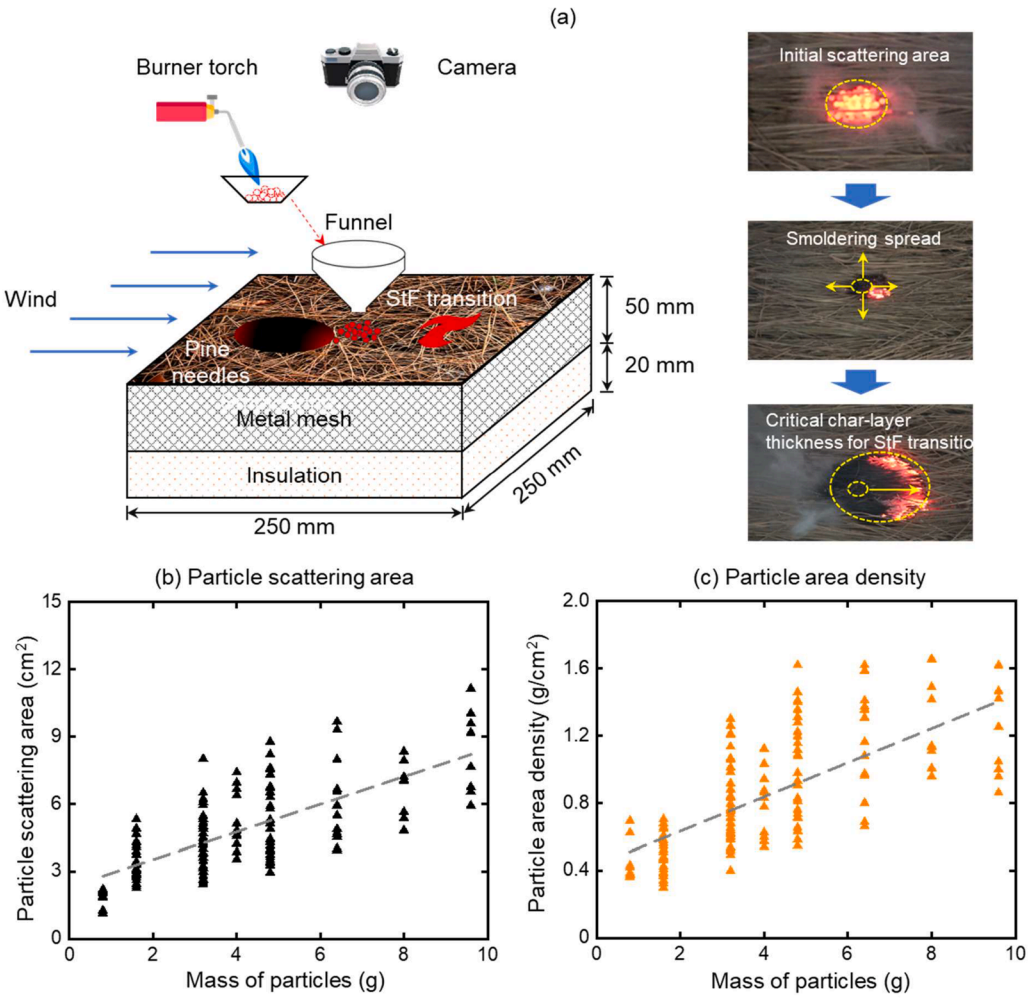

Fig. 1. Schematic of (a) experimental setup for multi-hot particle ignition of pine needle, and (b) particle scattering area and (c) particle area density versus particle mass.

Table 1
Particle number, mass, and landing characteristics of 2-mm-diameter hot steel particles.

No. of 2-mm particles (#)	Total mass (g)	Equiv. Dia. of one particle (mm)	Initial scattering area (cm^2)	Spotting mass area density (g/cm^2)
25	0.8	4.5	1.8 ± 0.4	0.5 ± 0.1
50	1.6	6.3	3.4 ± 0.9	0.5 ± 0.1
100	3.2	9.3	4.3 ± 1.3	0.8 ± 0.2
125*	4.0	10	5.3 ± 1.3	0.8 ± 0.2
150	4.8	10.6	5.4 ± 1.7	1.0 ± 0.3
200	6.4	11.7	6.0 ± 1.8	1.1 ± 0.3
250	8.0	12.6	6.7±1.3	1.2±0.3
300	9.6	13.4	8.4±1.9	1.2±0.3

*Similarly, 250 and 375 2-mm particles are equivalent to two and three 10-mm particles.

behavior under the present heating condition (~980°C). Subsequently, a 1.6-cm-diameter funnel positioned 0.5 cm above the bed was used to ensure a consistent release height and release location for the particles during deposition while minimizing dispersion during falling. After particle deposition, the funnel was promptly removed to minimize airflow disturbance. The measured temperature was used mainly to ensure consistent initial heating conditions across tests, rather than to determine the exact temperature of individual particles. Further characterization of particle surface temperature during release will be addressed in future work.

An axial-flow fan (SF4-4 Type) was turned on before particle release to establish the desired airflow, and its speed was controlled by the power-supply frequency from 0 - 50 Hz with a resolution of 0.1 Hz. Wind speed was measured using a calibrated portable anemometer (TS 9545). Before each test, the airflow was checked at the centerline and 2 cm above the fuel-bed surface to ensure both accurate and repeatable airflow conditions. An airflow of 2 m/s was applied to study the effects of particle number and fuel-bed moisture, while the airflow was adjusted in the range of 0.5–8 m/s when investigating wind speed effects. For each experimental run, the airflow was kept constant throughout the test. Because it is difficult to guarantee strictly laminar flow above the fuel bed in a laboratory setup, the present study focused on maintaining a stable and comparable forced-flow condition rather than characterizing a laminar boundary layer. Due to the complexity and randomness in both fuel and experimental conditions, 5 to 8 repeated trials were conducted for each condition to quantify the influence of particle number and scattering area on experimental outcomes. The ignition process was recorded at 50 frames per second by a video camera positioned at a 45° top-view angle, ensuring the fuel bed edge remained visible for analysis.

The scattering area of the particle spray on the fuel bed was measured automatically by MATLAB, with undetected cases outlined manually. Its calculation involved applying a perspective correction to account for the 45° viewing angle and thus enable accurate measurement of the initial scattering area of the deposited particles. The

particles consistently formed a single contiguous cluster rather than separate particle groups. The scattering areas measured in each repetition are shown as individual data points in Fig. 1(b) and Table 1, based on data from all experimental trials.

The average particle area density presented in Fig. 1(c), was used to indirectly characterize the concentration of deposited particles and their potential contact/exposure intensity on the fuel bed surface. By relating the total deposited mass to the measured scattering area, it also provides an approximate representation of the effect of inter-particle gaps, although it inevitably averages out localized variations caused by particle stacking or local clustering. Given the complexity and irregularity of natural deposition patterns, the present study adopts the initial particle distribution after release as a practical descriptor for analysis and focuses on its first-order influence on smoldering initiation, rather than further isolating the geometric effects of inter-particle spacing. The dotted lines in Fig. 1(b-c) are fitted trend lines for the experimental data, showing the overall linear dependence of particle distribution area and area density on particle mass. Accordingly, and these two experimentally obtained parameters were adopted as the primary descriptors of particle deposition for analyzing their influence on ignition.

3. Experimental results and discussion

3.1. Ignition phenomena of multi-particles

The observed ignition phenomena from multiple particles can be categorized as direct ignition, StF transition, and no ignition. This section first presents the observed ignition modes, followed by the ignition limits and their dependence on fuel and environmental conditions. All observed StF transitions occurred under environmental wind. Fig. 2(a) shows a sequence of images illustrating a typical StF ignition event in a pine needle fuel bed with a MC of 45%, under a 2 m/s wind and sprayed with 200 2-mm particles (energy equivalent to an 11.7 mm particle). The corresponding 45° top-view video is available in Supplementary Videos S1. The time of first particle contact with the fuel bed was defined as t = 0. All 200 particles were fully dispersed within 2 s. Upon landing, visible smoke, likely consisting of water vapor and pyrolysis gases, was emitted from the fuel bed and particles. The particles landed within an initial scattering area of 6.8 cm^2, which was 216 times of the cross-section area of a single particle and equivalent to a circular area with a diameter of $D_o = 2.9$ cm.

After particles gradually embedded into the porous fuel bed under gravity, smoldering fire was initiated. After 68 s, an unstable flash flame appeared, which was also corroborated by a transient increase in the spread rate shown in Fig. 3(a), where representative smoldering-spread phenomena are illustrated through the concurrent and opposed spread rates. The smoldering front exhibited a nearly circular pattern radiating outward from the cluster of hot particles, rather than propagating solely downwind as reported in previous studies [17]. Here, the concurrent spread rate refers to the smoldering spread rate in the wind direction, while the opposed spread rate refers to the smoldering spread rate against the wind direction. Such opposed smoldering spread faster than concurrent spread only occurred under a small wind. As burning area grew, the smoldering rate increased, eventually transitioning to flaming at 451 s, by which time the smoldering area had reached 132 cm^2 ($D_{sm} =$ 13 cm). The resulting flame propagated until the burnout of fuel bed.

When the fuel is further oven-dried after air drying (MC = 5%), Fig. 2 (b) shows a similar ignition process of StF transition with 100 2-mm

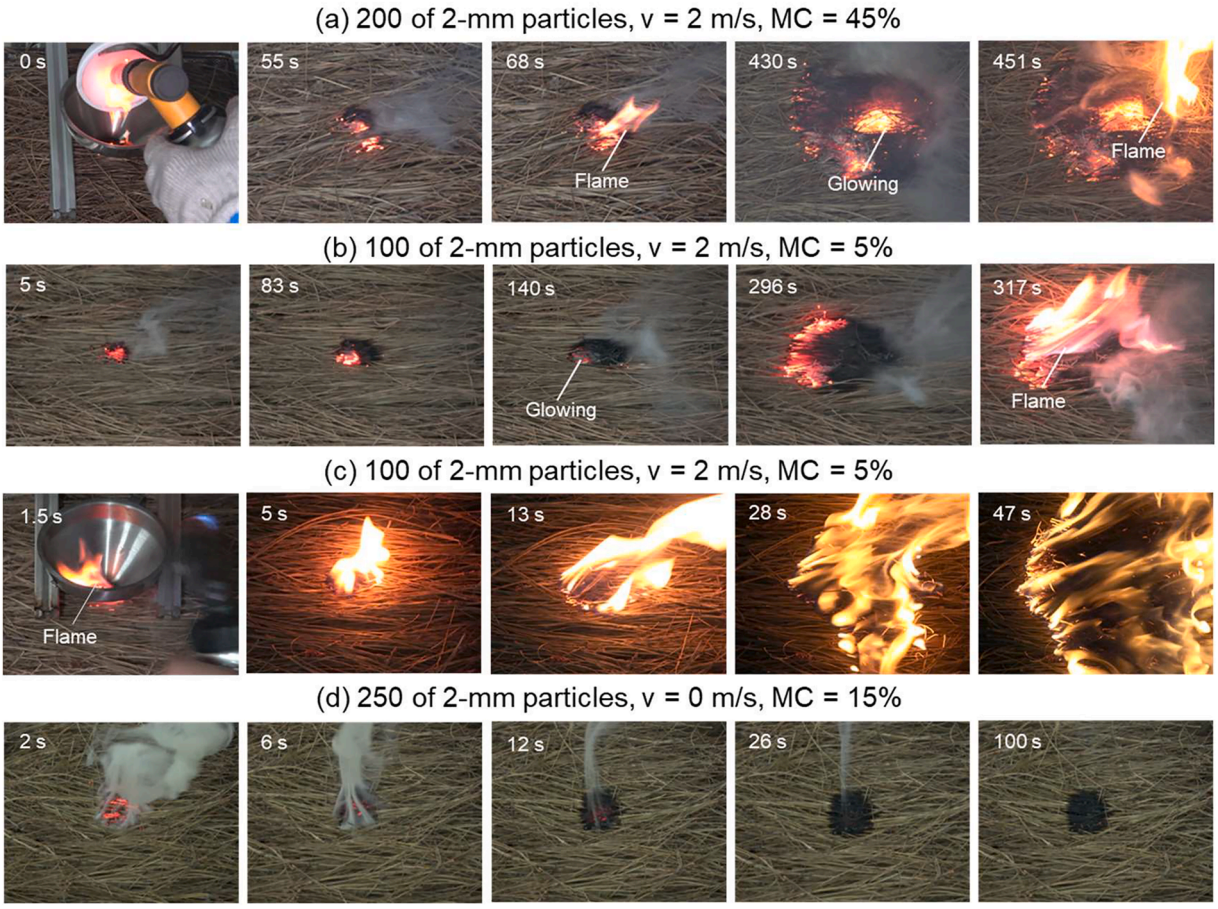

Fig. 2. Snapshots of the hot-particle ignition processes in pine needles: (a-b) StF transition with 2 m/s wind, (c) direct flaming ignition, and (d) smoldering ignition without flaming in no wind.

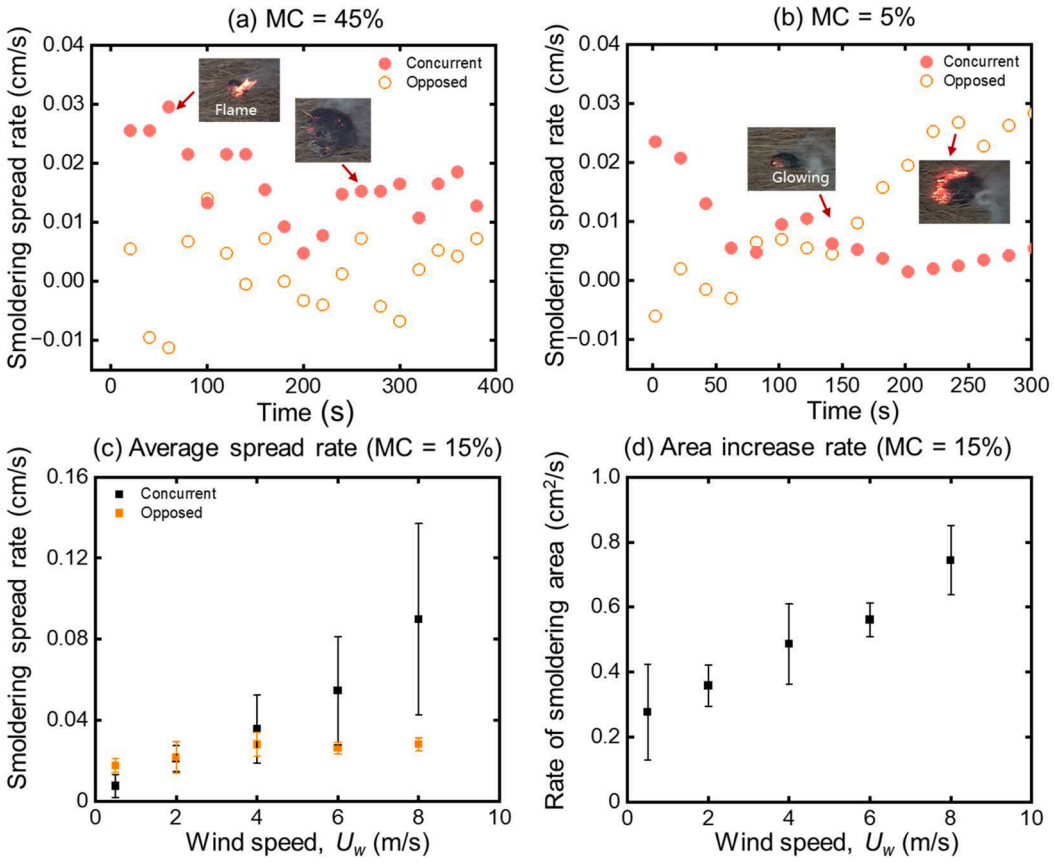

Fig. 3. Both concurrent and opposed smoldering spread rates in pine needles: StF transition under a 2 m/s wind with (a) MC of 45% and sprayed with 200 2-mm particles, (b) MC of 5%, and sprayed with 100 2-mm particles, (c) smoldering spread rates and (d) growth of smoldering area with a MC of 15% and sprayed with 125 particles (2-mm diameter) under different winds.

particles. Compared to the ignition of wetter fuel bed in Fig. 2(a), stronger smoldering ignition and spread phenomena occurred between 5 and 317 s. The particles were scattered in approximately 1 s, forming an initial scattering area of about 5.2 cm^2 ($D_o = 2.6$ cm). Between 80 s and 150 s in Fig. 3(a), the concurrent and opposed spread rates were comparable, while beyond 150 s, the opposed spread rate exceeded that in the concurrent direction. This is attributed to the fact that the nearly circular smoldering front observed between 80 s and 140 s began to exhibit glowing on the left side of the fuel bed (i.e., the opposed-wind direction relative to particle landing position) at 147 s, which progressively enhanced smoldering spread in the opposed direction. After 100 s, the left side of the fuel bed began to exhibit glowing combustion due to earlier oxygen availability, progressively enhancing the opposed smoldering spread rate. At the transition to flaming, the observed smoldering area reached about 52 cm^2 ($D_{sm} = 8$ cm). This area represents a 61% decrease, compared to the 132 cm^2 ($D_{sm} = 13$ cm) measured in Fig. 2(a), indicating that lower moisture content substantially reduces the effective smoldering area at the transition to flaming and accelerates the StF transition dynamics.

Fig. 2(c) demonstrates direct flaming ignition under identical initial conditions of Fig. 2(b). Frame-by-frame video analysis revealed a visible, sustained flame on the fuel bed surface approximately 1 s after the first hot particle landed. This flame then propagated rapidly, dominating the fire spread and fuel consumption across the entire bed. This ignition mode occasionally occurs when multiple hot particles ignite fuel bed with a low moisture content.

When the wind speed decreased to 0 m/s, even the 250 of tiny 2-mm particles (with energy equivalent to two 10-mm particles) were sprinkled onto a fuel bed with a MC of 15% in Fig. 2(d). The particles were released at approximately 1 s, and their descending and smoldering ignition behavior were similar to that under wind scenarios of Fig. 2(a-c). Under no-wind conditions, only a brief and localized smoldering phenomenon (i.e., smoke release and limited surface charring) was observed; however, it did not evolve into self-sustained smoldering spread or flaming ignition, and was therefore classified as an unsuccessful ignition. This contrasts with the flaming ignition and StF transition observed in wind-affected scenarios of Fig. 2(a-c), highlighting the critical role of the forced wind in promoting rapid glowing or transition from smoldering to flaming.

Noticeably, unlike the previous studies involving a single large hot inert particle [17] or a small number of firebrand (piles) [16,23], no sustained smoldering ignition was observed in this work. Ignition by multi-particle clusters typically led to complete consumption of the fuel bed, whereas a single large hot inert particle consumed more than half but not all of the fuel bed [17]. Since the result in Ref. [17] was obtained under the same fuel MC and airflow conditions as those used here, this difference is attributed to the significantly larger ignition area produced by multi-particle clusters compared to that from a single particle of equivalent energy. Consequently, once ignited, multi-particle clusters result in more extensive fire spread and burning than a single particle of the same total energy.

3.2. *Ignition limit of multi-particle spotting*

In direct flaming and StF transition cases, the emergence of a sustained flame dominated fire spread and consumed nearly the entire fuel bed. From these observed outcomes, the ignition criterion was defined and then used to determine the ignition limit of multi-particle spotting. Here, ignition (°) refers to mass loss percentage $>$ 95%, whereas no ignition (×) refers to mass loss percentage $<$ 5%. Fig. 4a summarizes

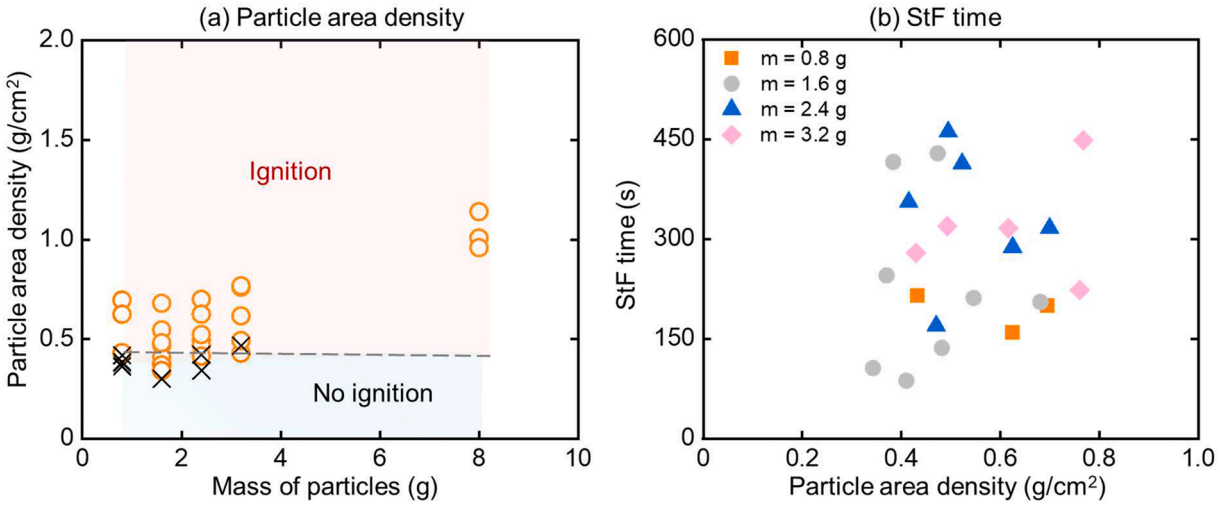

Fig. 4. Effect of multiple-particle mass and area density on (a) ignition outcome and (b) ignition delay time via StF transition of dry fuel with MC of 5% and an environmental wind of 2 m/s.

these outcomes under a MC of 5% and a 2 m/s wind, across varying multi-particle masses and initial particle area density. Each point represents one test, and the ignition threshold for initial particle area density is marked with a grey dashed line. The ignition threshold broadens slightly with increasing particle mass, whereas the critical particle area density for ignition stays constant at around 0.4 g/cm^2. Because the particles were released from the same location, the main deposition area remained broadly similar across tests. As particle number increased, more particles accumulated within a comparable area, leading to a more compact distribution and a higher particle area density. As a result, the higher-mass cases were generally above the critical density range, and no near-threshold cases were observed.

For a given particle mass, a more localized dispersion area is more prone to successful ignition. Taking the hot particles of the same mass

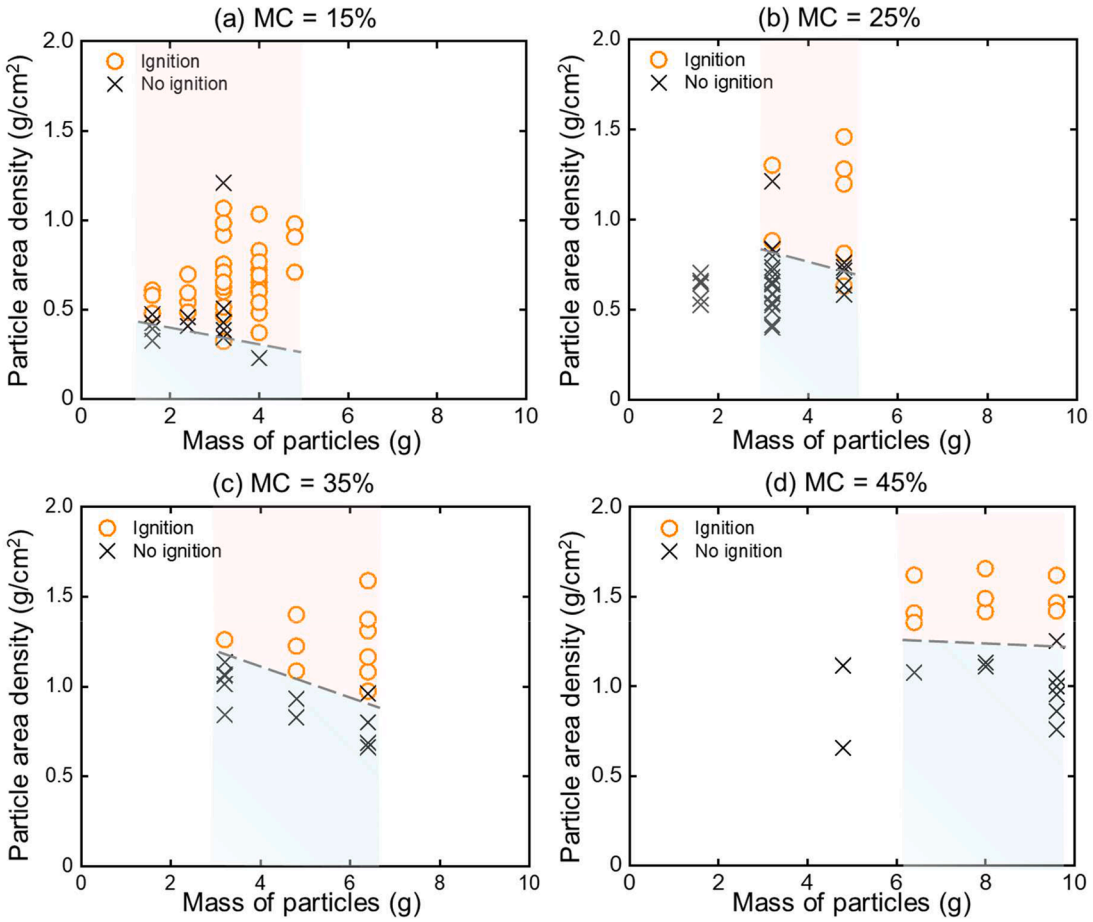

Fig. 5. Effects of moisture contents on the experimental outcomes of ignition (°) and no ignition (×) under varying conditions of multi-particle mass and initial particle area density, with an environmental wind of 2 m/s.

(25 2-mm particle) as example, the ignition occurred when the particle area density was 0.6 ± 0.1 g/cm^2, whereas no ignition was observed when the particle area density was 0.40 ± 0.02 g/cm^2. This suggests that accumulated particles are more likely to ignite the fuel than distributed ones, perhaps due to reduced cooling rates of the accumulated particles.

To quantify the initiation of multi-particle ignition, the ignition delay time is defined as the period from the arrival of the first hot particle on the fuel bed to the appearance of flame. The measured delay times for StF transition are plotted as a function of initial particle area density and total mass of hot particles in Fig. 4(b), under dry fuel conditions (MC of 5%) and an ambient wind speed of 2 m/s. The results indicate that the ignition delay time exhibits no clear dependence on the particle area density across different masses of hot particles. These findings demonstrate that, for the ignition of a pine needle bed by multiple hot particles, the delay time is independent of both the particle mass and their spatial distribution. Instead, the delay is primarily determined by the location and extent of the resulting glowing smoldering region, as illustrated in Fig. 2(b). A large glowing zone initiated on the surface of the fuel bed undergoes a rapid transition to flaming due to sufficient oxygen supplement. In contrast, a glowing zone formed internally within the fuel bed significantly prolongs the ignition delay.

3.3. Effect of moisture content on the ignition limit

After defining the ignition limit, the effect of fuel properties is examined, with particular focus on moisture content. The influence of moisture content on the experimental outcomes of ignition (°) and no ignition (×) with an environmental wind speed of 2 m/s, under varying conditions of multi-particle mass and initial particle area density, is summarized in Fig. 5. For each MC level, a consistent relationship is observed between the critical initial particle area density and the multi-particle mass: ignition occurs with smaller multi-particle masses when the particle distribution is more concentrated (larger particle area density), while for larger quantities, ignition can be achieved over a wider range of particle area density. This behavior is attributed to inter-particle heat transfer within clusters, which reduces the cooling rate of individual particles and thus increases the likelihood of ignition.

An anomaly was observed at a particle mass of 3.2 g and an initial particle area density of 1.2 g/cm^2, where ignition failed. In this case, the particles remained mostly on the fuel-bed surface due to a compact arrangement, causing extended surface cooling and reducing effective heating to the underlying fuel. In typical cases, however, particles embed into the fuel bed under gravity, enhancing heat transfer and increasing ignition probability. These findings emphasize the complex relationships among particle distribution, thermal behavior, and fuel properties in multi-particle ignition. As shown in Fig. 5(a-d), higher moisture content requires a greater total particle mass and a larger particle area density to achieve ignition. In other words, the critical area density for ignition is more dependent on the moisture content than on the particle mass. This phenomenon results from the fact that elevated fuel moisture content demands more energy to compensate for the heat consumed by water vaporization, thereby increasing the minimum energy required for ignition.

In order to better quantify the effect of moisture content, Fig. 6 illustrates its influence on experimental outcomes of ignition (°) and no ignition (×) at constant masses of 4.8 g, as well as the ignition delay time at constant masses of 4.8 g or 6.4 g (corresponding to 150 or 200 hot 2-mm metal particles). The increase in moisture content directly elevates both the energy and time required for ignition, thereby narrowing the range of conditions that result in successful ignition. Beyond a critical MC threshold (e.g., 35% in this case), the limited thermal energy from the hot particles becomes insufficient to simultaneously meet the competing requirements of water evaporation and fuel pyrolysis, ultimately leading to no ignition.

Furthermore, at a MC of 35%, the average delay time for the 6.4 g particle mass is shorter than that for the 4.8 g mass, indicating that an increase in particle mass can lead to a reduction in delay time under this specific condition, evidenced by comparing the constant masses of 4.8 g (red triangles) and 6.4 g (purple squares). This behavior can be attributed to the role of hot-particle ignition in forest fuel beds, which acts primarily as a heating source to initiate self-sustaining smoldering. Consequently, the StF transition time increases with higher moisture content.

3.4. Effect of airflow on the ignition limit

The effect of environmental conditions is then examined, with emphasis on airflow. Fig. 7(a) summarizes the effects of varying wind speeds (0.5, 2, 4, 6, and 8 m/s) on the ignition (°) and no ignition (×) outcomes and smoldering spread rate for 125 hot particles under various initial particle area density with a moisture content of 15%. At a wind speed of 0.5 m/s, multi-particles ignition only occurred when the particles were densely concentrated (initial particle area density > 0.7 g/cm^2). As the wind speed increased, the successful ignition was observed over a broader range of particle area density. This trend is attributed to the enhanced mixing between air and pyrolysis gases, which promotes

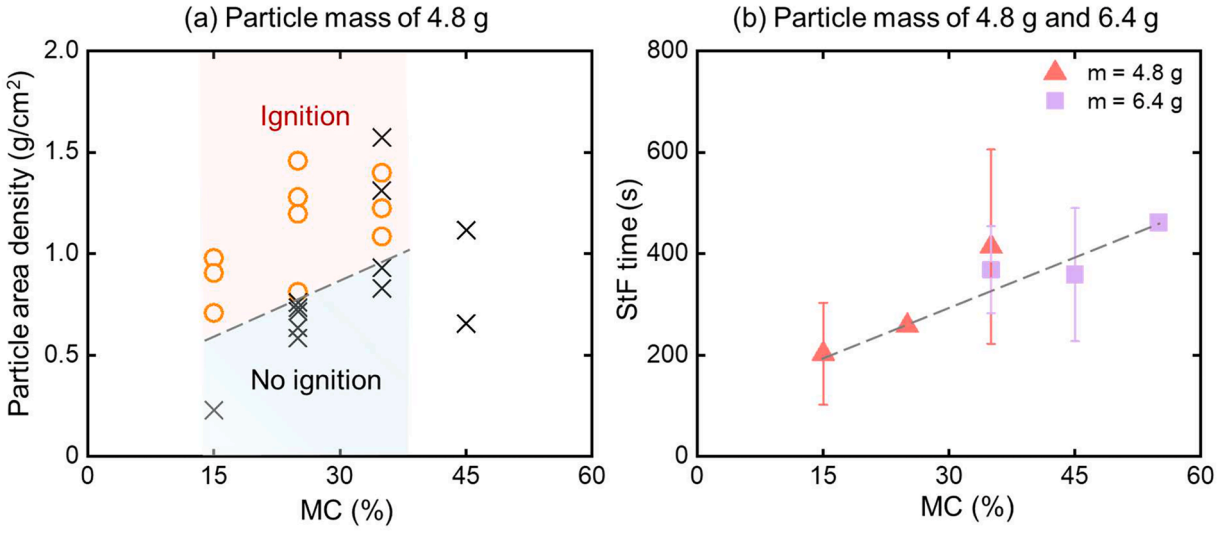

Fig. 6. Effect of MC on the (a) experimental outcomes of ignition (°) and no ignition (×) at constant masses of 4.8 g, and (b) ignition delay time at constant masses of 4.8 g and 6.4 g, with 2 m/s wind.

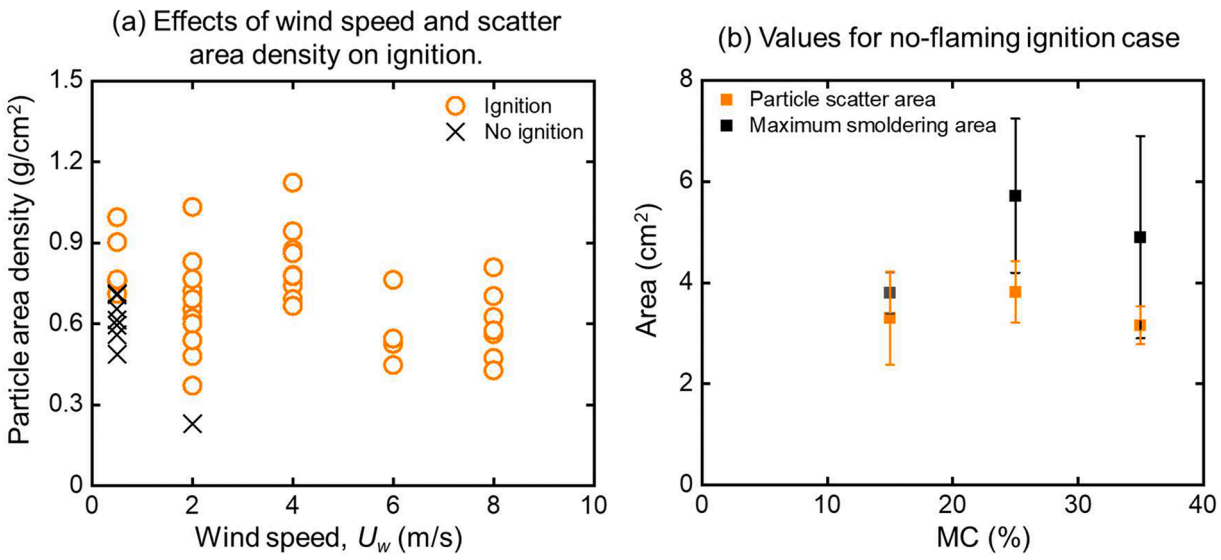

Fig. 7. Effects of (a) varying wind speeds and particle area density on the ignition (°) and no ignition (×) outcomes for 125 hot particles with a moisture content of 15% and (b) MC on the maximum smoldering area and initial scatter area of no ignition case for 100 hot particles and 2 m/s wind.

smoldering propagation and ignition.

When the wind speed is at the range of 0.5 to 2 m/s, the rate of opposed smoldering spread rate is larger than that of concurrent smoldering spread, as visualized in Fig. 2(b) and further compared in Fig. 3 (c). At higher wind speeds (4, 6, and 8 m/s), the spread rate becomes greater in the concurrent direction. As the wind speed increases, the concurrent spread rate rises linearly, while the opposed spread rate stabilizes at 0.03 cm/s. Overall, the expansion rate of the smoldering front is enhanced by increasing wind speed in Fig. 3(d). This suggests that an insufficient oxygen supply at the concurrent direction, and the cooling effect of the wind may outweigh the effect of enhanced oxygen supply under these conditions. Notably, the ignition probability is 50% at the wind speed of 0.5 m/s, while it is 100% across the reaming range, suggesting that the ignition process is mainly determined by the forward smoldering.

Fig. 8 illustrates the influence of the initial dispersion area on the ignition delay time for a constant mass of 4.0 g (125 hot 2-mm particles) under various wind speeds. It should be noted that a wind speed of 8 m/s is insufficient to displace the 2-mm-diameter hot particles and thus does not significantly alter their distribution. In wind-assisted environments, the ignition delay time of a pine needle fuel bed ignited by multiple hot particles exhibits a strong negative correlation with environmental wind speed, while showing no significant association with the initial scattering area of the hot particles. This indicates that wind-driven convective heat and mass transfer are the dominant mechanisms governing the transition from smoldering to flaming, outweighing the initial geometric distribution of the heat source.

Within the wind speed range of 0 to 8 m/s, the multi-particles ignition delay time of a pine needle fuel bed decreases rapidly as the wind speed increases, reaching the minimum value (in the O_2 -limited Regime). This trend is consistent with experimental observations reported in [17]. The reduction in ignition delay is ascribed to the enhanced oxygen supply and improved mixing of combustible gases, which significantly accelerate smoldering propagation and shorten the transition from smoldering to flaming. However, when the wind speed exceeds approximately 4 m/s, which marks an empirical transition point under the present experimental conditions rather than a universal critical wind speed, the ignition delay time stabilizes at 140 ± 59 s across a broad range of airflow velocities, indicating a shift to the thermal regime. In this regime, the oxygen supply is no longer the rate-limiting

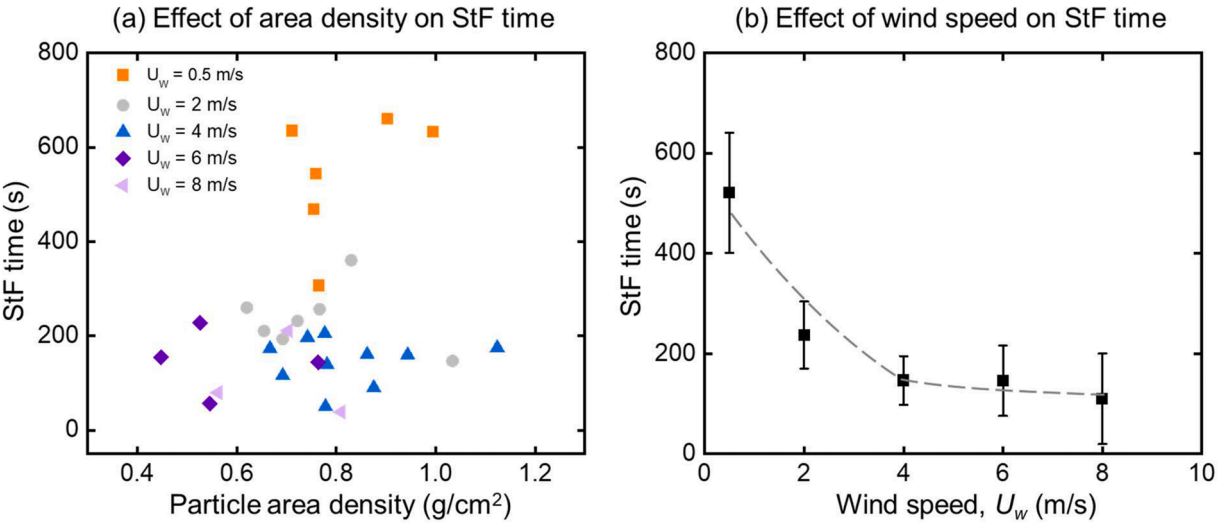

Fig. 8. Influence of airflow on the (a) initial particle area density and (b) ignition delay time for a constant mass of 4.0 g (125 hot 2-mm particles).

factor for the StF transition or the smoldering propagation rate. Instead, internal thermal conduction within the fuel becomes the dominant factor controlling the transition process, while the increasing convective cooling effect begins to offset the promoting effect of airflow. Although not observed in the current experiments, a further increase in wind speed is expected to lead to a slight prolongation of the ignition delay time, referred to as the chemical regime, until eventual blow-off occurs. In this regime, the cooling effect of the airflow on char oxidation can no longer be neglected.

4. Theoretical Analysis of Ignition Limit

4.1. Maximum heating efficiency of multi-particle

In the aforementioned experiment, multi-particle ignition can be regarded as the process of depositing and heating a thin cylinder with a surface area (A) of 1 - 16 cm^2 and a thickness (δ) of 2 - 6 mm. Due to a small Biot number (Bimax~0.01<<1), the effective heating or the self-cooling time of the multi-particle (t_h) can be estimated using the lumped capacity method as

$$\rho V c_p \frac{dT}{dt} \approx -A h_c (T - T_a) \tag{1}$$

The parameters containing the symbols, their physical meanings, units, and typical values in the calculation have been listed in Tab. 2.

Because of the randomness of each test and the fuel bed, the heat transfer process between the particle cluster and the fuel bed is different to described in detail. To simply this process, the distribution of particles is assumed to be uniform within the scatter area and is further simplified as a flat plate. As a primary heating source for the hot-particle ignition to initiate a self-sustaining smoldering process in forest fuel beds, the temperature variable in Eq. 1 is integrated from its initial value (T_p) to the minimum effective heating temperature ($\cong T_{sm} \gg T_a$) to describe the thermal evolution during the hot-particles ignition process as:

$$\frac{T_{sm}}{T_p} \approx \exp\left(-\frac{2h_c A}{\rho c_p V} t_h\right) \approx 1 - \frac{2h_c A}{m c_p} t_h \tag{2}$$

Then, the effective heating time from its initial temperature (T_p) to the minimum effective heating temperature (T_{sm}) can be estimated as

$$t_h \approx \frac{m c_p}{2h_c A}\left(1 - \frac{T_{sm}}{T_p}\right) \tag{3}$$

Where m is the mass of particles, A is the scattered-particle area, c_p is the specific heat of the particle, and h_c is the overall cooling coefficient accounting for cooling by both the fuel bed and the environment. Here, taking the minimum effective heating temperature (T_{sm}) as 500°C [32, 38] and the initial temperature (T_p) as 980°C. As shown in Fig. 9a, the effective heating time (or the cooling duration) of the particle decreases with the increasing secreted area, much longer than that of a single 2-mm particle (1.97 s), at a wind speed of 2 m/s. During the cooling of particles, the fuel bed is also heated by these hot multi-particles. At the end of heating ($t = t_h$), a fuel layer within a short distance l_h from the multi-particle is heated to T_{sm}. Such a heating process can be described through a simplified one-dimensional heat equation as follows:

$$k_f \frac{\overline{T}_p - \overline{T}_f}{l_h} t_h = l_h \rho_f \left(c_f T_{sm} + \mathrm{MC}\Delta H_{ev}\right) \tag{4}$$

where k_f is the effective thermal conductivity of fuel bed, $\overline{T}_p = (T_{p0} + T_{sm})/2$ and $\overline{T}_f = (T_{sm} + T_a)/2 \gg T_a$. Then, we can estimate this heating distance, i.e. the characteristic char-layer thickness generated by the particle heating, as

$$l_h = \sqrt{\frac{k_f T_p t_h}{2\rho_f (c_f T_{sm} + \mathrm{MC}\ \Delta H_{ev})}} = \sqrt{\frac{k_f m c_p (T_p - T_{sm})}{4h_c A \rho_f (c_f T_{sm} + \mathrm{MC}\ \Delta H_{ev})}} \tag{5}$$

where $\rho_f = 40$ kg/m^3, $k_f \approx 0.05$ W/m-K, and $c_f = 1200$ J/kg-K for fuel bed are used in the calculation. The calculated heating length (l_h) clearly decreases with MC in Fig. 9(a). Meanwhile, for the same particles cluster mass, larger scattered area resulting in the shorter t_h.

Then, based on heat-transfer principles, an overall heating η_0 can be defined as:

$$\eta_0 = \frac{\text{Energy absorbed by fuel}}{\text{Total particles energy}} = \frac{l_h A_p \rho_f (c_f T_{sm} + \mathrm{MC}\Delta H_{ev})}{\rho_p V_p c_p T_p} \tag{6}$$

where $\Delta H_{ev} = 2.26$ MJ/kg is the latent heat of vaporization of water [45]. A large amount of energy is not necessary to ignite the fuel if the particles are not hot enough. Therefore, effective energy (η_{sp}) is a more useful and physically meaningful parameter to estimate the ignition risk, which can be defined as[17]:

$$\eta_{sp} = \frac{\text{Energy absorbed by fuel}}{\text{Total energy of particles}} = \frac{l_h A_p \rho_f (c_f T_{sm} + \mathrm{MC}\Delta H_{ev})}{\rho_p V_p c_p (T_p - T_{sm})} \tag{7}$$

Fig. 9(b) shows the calculated results of l_h and η_{sp} as a function of particles mass with $A = 6$ cm^2 and MC = 15% at a wind speed of 2 m/s. The results indicate that the cluster with lower mass exhibit higher heating efficiency at the same temperature and scattered area. However, due to rapid convective cooling and reduced total energy, the temperature decreases quickly, leading to a significant drop in l_h. During this cooling process, the reaction front of the fuel must reach a threshold thickness to maintain self-sustaining smoldering combustion, otherwise the glowing will eventually gradually extinguish. According to the experiment, the critical particles mass is approximately 2.4 g ($P_{ig} = 66\%$) with $A = 6$ cm^2 corresponding to a calculated critical thickness $l_h = 1.34$ cm.

Table 2
List of symbols, physical meaning, units, and typical values.

Symbol	Physical Meaning	Unit	Typical Value / Range
m	Total mass of multi-particles	g	0.8 – 9.6 g
A	Initial scattering area of multi-particles	cm^2	1 – 16 cm^2
ρ_p	Density of stainless-steel particles	kg/m^3	7687 ± 7 kg/m^3
c_p	Specific heat capacity of steel particles [17]	J/(kg·K)	500 J/(kg·K)
T_p	Initial particle temperature	°C	980 ± 20°C
T_{sm}	Minimum effective heating temperature [40,43]	°C	500°C
h	Overall convective cooling coefficient	W/(m^2·K)	195 W/(m^2·K)
Bi	Biot number of multi-particle cluster	–	≈0.01 (Bi < 0.1)
t_h	Effective heating (cooling) time of particle	s	2 – 50 s depending on A and m
k_f	Effective thermal conductivity of fuel bed [17]	W/(m·K)	≈0.05 W/(m·K)
ρ_f	Bulk density of pine needle fuel bed [17]	kg/m^3	40 ± 5 kg/m^3
c_f	Specific heat of pine needles [17]	J/(kg·K)	≈1200 J/(kg·K)
ΔH_{ev}	Latent heat of water vaporization [44]	J/kg	2.26 × 10^6 J/kg
l_h	Heating depth (char-layer thickness)	cm	0.1 – 1.5 cm
$\dot{s}$	Smoldering spread rate	cm/s	0.01 – 0.2 cm/s
v	Wind speed	m/s	0 – 8 m/s
MC	Fuel moisture content	% (dry basis)	5 – 45%
η_{sp}	Heating efficiency of multi-particles	–	0 – 1
$t_{sm,f}$	Ignition delay time (StF transition)	s	≈30 – 650 s

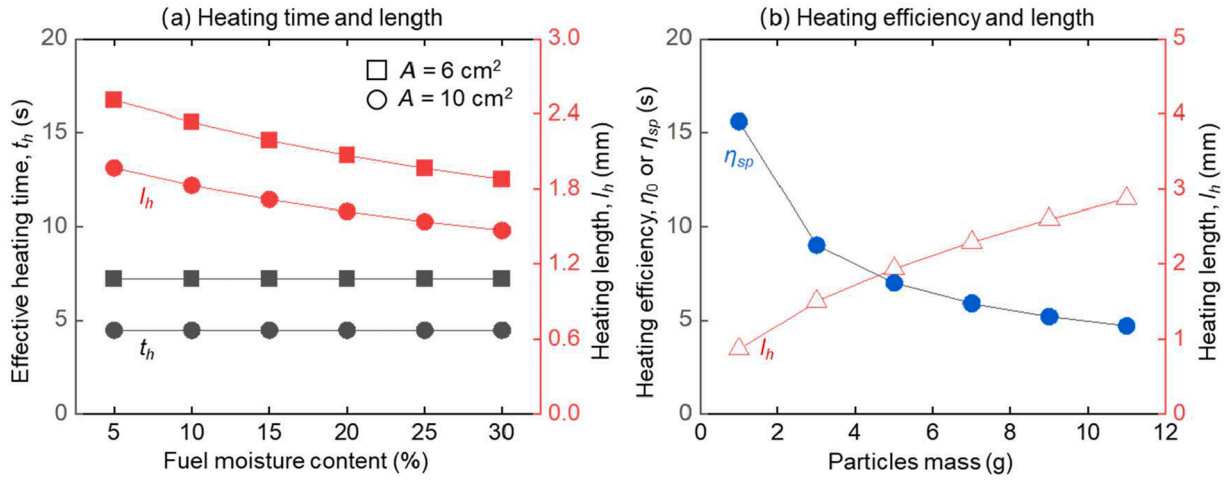

Fig. 9. (a) Estimated effective heating time (t_h) and length (l_h) of particle as a function of fuel moisture content (MC) with m = 6.4 g; and (b) specific heating efficiency (η_{sp}) of particle and length (l_h) as a function of particles mass with A = 6 cm and MC = 15%.

4.2. Airflow effect on the smouldering-to-flaming transition

The delay time for StF transition can be very long, and has been observed to last from a few minutes (as shown in Figs. 3, 5, 7) to several hours [32], depending on the fuel properties, fire conditions and environmental factors. Based on the observations in the literature, this transition can be hypothesized to result from a spontaneous ignition after the mixing of pyrolysis gases with preheated air. The air is preheated by highly exothermic secondary char oxidation within a thick char layer. As the char layer thickens, the charring zone becomes more likely to initiate secondary char oxidation, thereby providing a longer residence time for air preheating. Consequently, the thickness of the self-sustained char layer plays a critical role in enabling StF transition [17,33,34]. To quantify this process, a critical char-layer thickness (l_{crt}) is introduced as the key criterion for transition. As illustrated in Fig. 10 (a), this critical char-layer thickness (l_{crt}) is initially generated by the direct heating from the hot particle (l_h), followed by the self-sustained smoldering spread (l_s):

$$l_{crt} = l_h + l_s = V_p t_h + V_{sm} t_{sm} \tag{8}$$

For a fixed fuel bed under given environmental conditions, l_{crt} can be considered constant. Thus, the delay time of StF transition can be determined as follows:

$$t_{sm,f} = t_h + t_{sm} = t_h + \frac{l_{crt} - l_h}{V_{sm}} \tag{9a}$$

where t_h and l_h are obtained from the particle heating model (Eqs. 3 and 5), while the self-sustained smoldering spread rate (V_{sm}) depends solely on fuel properties and wind, independent of the hot particles. Substituting Eqs. 3 and 5 into Eq. 9a yields:

$$t_{sm,f} = t_h + t_{sm} = \frac{mc_p}{2h_c A}\left(1 - \frac{T_{sm}}{T_p}\right) + \frac{1}{V_{sm}}\left[l_{crt} - \chi\left(T_p - T_{sm}\right)^{1/2}\right] \tag{9b}$$

with

$$\chi = \sqrt{\frac{k_f m c_p}{4h_c A \rho_f \left(c_f T_{sm} + \mathrm{MC}\ \Delta H_{ev}\right)}} \tag{10}$$

which is related to the fuel and particle clusters properties as well as the wind condition, but is independent of the particle temperature and size.

Equation (9b) indicates that the smouldering phase duration (t_{sm}) decreases with increasing initial temperature. More importantly, the

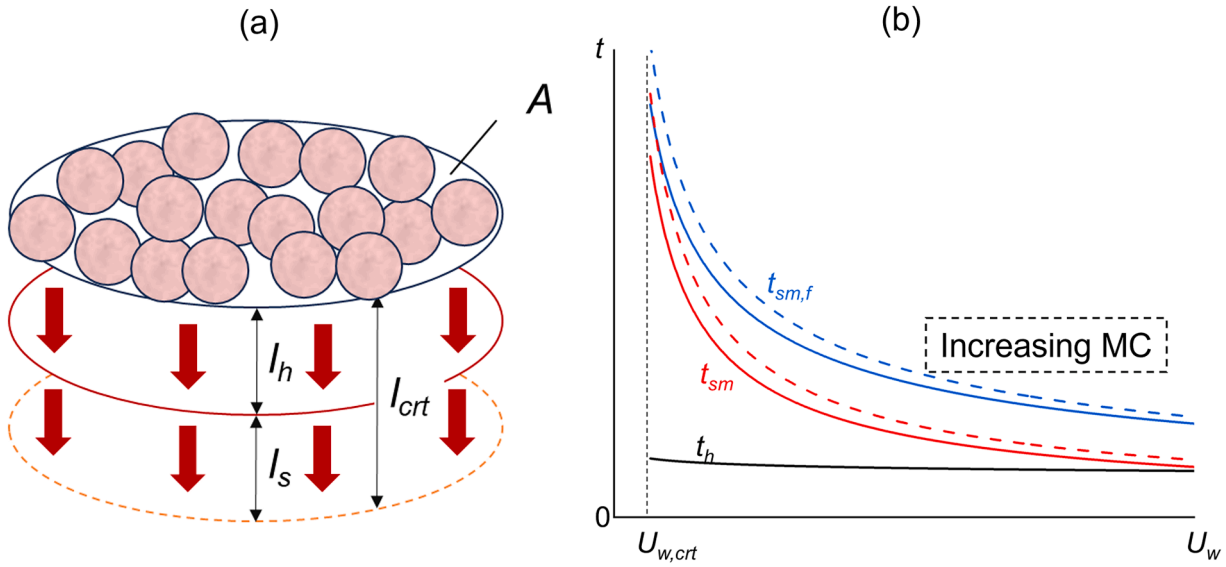

Fig. 10. (a) Illustration of the smoldering process before the transition to flaming; and (b) StF ignition delay time ($t_{sm,f}$) varying with the wind speed.

smouldering spread rate (V_{sm}) over pine needle bed, is known from literature to depend on the fuel moisture (MC) and wind speed (U_w), with $V_{sm} \propto MC^{-1/2}$ and $V_{sm} \propto U_w$ [40,46]. These dependencies provide a direct link between environmental conditions and the observed delay times: As wind speed increases, V_{sm} rises, shortening $t_{sm,f}$ explaining the rapid decrease in delay time with wind speed shown in Fig. 8(b). As moisture content increases, V_{sm} decreases, lengthening $t_{sm,f}$ which aligns with the increasing delay time trends in Fig. 6(b). Fig. 10(b) qualitatively illustrates the variation of $t_{sm,f}$ with wind speed as predicted by Eq. 9b. The curve captures the experimental trend well: a rapid decrease in delay time at low winds (oxygen-limited regime), followed by stabilization at moderate winds (thermal regime) [47]. The model also suggests the existence of a low critical wind speed below which the StF transition may not occur due to insufficient oxygen supply—consistent with the low ignition probability observed at 0.5 m/s in Fig. 7(a).

In summary, the proposed critical char-layer thickness model provides a coherent framework explaining how wind speed and fuel moisture affect the StF transition delay during multi-particle ignition. While the model does not aim to provide precise quantitative predictions for all scenarios which would require more complex multi-dimensional simulations, it successfully captures the key physical mechanisms and aligns with the experimental observations.

5. Conclusions

In this work, hundreds of 2-mm diameter stainless steel hot particles at 980 ± 20 °C have been deposited onto the pine needle bed with a moisture content (MC) of 5 - 45% and wind speed of 0 - 8 m/s. Several ignition phenomena including direct flaming, StF transition and no ignition were observed. The minimum particle area density of multiple hot particles was 0.4 g/cm^2 for the MC of 5%, and this value increased with higher MC. Compared with dispersed distributions, more clustered dispersion was found to promote ignition more effectively, owing to reduced environmental cooling and stronger inter-particle heating. This study further shows that particle area density serves as a more appropriate indicator of ignition hazard than total particle mass.

The StF ignition became easier and faster with the increased wind speed and the decreased fuel MC, where the opposed smoldering spread exceeds the concurrent spread under a small wind. Besides, the ignition delay of smoldering and StF transition was governed primarily by the location and extent of surface glowing and in-depth smoldering region, rather than by the total mass and spatial distribution of the particle group. A simplified heat transfer analysis is adopted to explain the spotting ignition threshold and delay time under different moisture and wind conditions based on a minimum char-layer thickness. This work enhances the understanding of the fire hazard associated with multiple hot-particle ignition, while its quantitative applicability is limited by the use of a single nominal particle temperature, the unresolved particle temperature evolution during release and falling, and the simplified treatment of particle deposition and particle-fuel contact conditions. Future work should therefore incorporate varied particle temperatures, particle spacing, and higher-fidelity multi-physics modeling to better represent realistic firebrand ignition scenarios.

CRediT authorship contribution statement

Supan Wang: Writing – original draft, Methodology, Formal analysis, Funding acquisition. **Wenhao Xu:** Investigation, Methodology, Formal analysis, Data curation. **Chunyin Zhang:** Resources, Investigation. **Xinyan Huang:** Writing – review & editing, Formal analysis, Conceptualization. **Carlos Fernandez-Pello:** Conceptualization, Writing – review & editing.

Declaration of competing interest

The authors declare that they have no known competing financial interests or personal relationships that could have appeared to influence the work reported in this paper.

Acknowledgements

SW thanks the support from the National Key R&D Program of China (No. 2023YFC3081600) and the National Natural Science Foundation of China (No. 52176113). XH thanks the support from the National Natural Science Foundation of China (No. 52322610) and PolyU Research Institute for Sustainable Urban Development (P0058005).

Supplementary materials

Supplementary material associated with this article can be found, in the online version, at doi:10.1016/j.jaecs.2026.100510.

Data availability

Data will be made available on request.

References

[1] Chen B, Wu S, Jin Y, Song Y, Wu C, Venevsky S, Xu B, Webster C, Gong P. Wildfire risk for global wildland–urban interface areas. Nat Sustain 2024;7:474–84. https://doi.org/10.1038/s41893-024-01291-0.
[2] Liu Y, Stanturf J, Goodrick S. Trends in global wildfire potential in a changing climate. For Ecol Manage 2010;259:685–97. https://doi.org/10.1016/j.foreco.2009.09.002.
[3] Ellis TM, Bowman DMJS, Jain P, Flannigan MD, Williamson GJ. Global increase in wildfire risk due to climate driven declines in fuel moisture. Glob Chang Biol 2022;28:1544–59. https://doi.org/10.1111/gcb.16006.
[4] Caton SE, Hakes RSP, Gorham DJ, Zhou A, Gollner MJ. Review of pathways for building fire spread in the wildland urban interface part I: exposure conditions. Fire Technol 2017;53:429–73. https://doi.org/10.1007/s10694-016-0589-z.
[5] Fernandez-pello AC. Wildland fire spot ignition by sparks and firebrands, Fire saf. J 2017;91:2–10. https://doi.org/10.1016/j.firesaf.2017.04.040.
[6] Liu N, Lei J, Gao W, Chen H, Xie X. Combustion dynamics of large-scale wildfires. Proc Combust Inst 2021;38:157–98. https://doi.org/10.1016/j.proci.2020.11.006.
[7] Manzello SL, Suzuki S, Gollner MJ, Fernandez-pello AC. Role of firebrand combustion in large outdoor fire spread. Prog Energy Combust Sci 2020;76:100801. https://doi.org/10.1016/j.pecs.2019.100801.
[8] Wang S, Thomsen M, Huang X. Spot ignition of a wildland fire and its transition to propagation. Int J Wildl Fire 2024;33:1–8. https://doi.org/10.1071/WF23207.
[9] Cahoon DR, Stocks BJ, Levine JS, Cofer WR, Pierson JM. Satellite analysis of the severe 1987 forest fires in northern China and southeastern Siberia. J Geophys Res Atmos 1994;99:18627–38. https://doi.org/10.1029/94jd01024.
[10] Link ED, Maranghides A. Burnover events identified during the 2018 Camp Fire. Internat J Wildl Fire 2023;32:989–97. https://doi.org/10.1071/WF22115.
[11] NSW Government - Premier & Cabinet, D. Owens. M. O'Kane, Final Report of the NSW Bushfire Inquiry. Dep Prem Cabinet 2020.
[12] Manzello SL, Maranghides A, Mell E, William. Firebrand generation from burning vegetation. Int J Wildl Fire 2007;16:458–62. https://doi.org/10.1071/WF06079.
[13] Manzello SL, Park SH, Suzuki S, Shields JR, Hayashi Y. Experimental investigation of structure vulnerabilities to firebrand showers. Fire Saf J 2011;46:568–78. https://doi.org/10.1016/j.firesaf.2011.09.003.
[14] Suzuki S, Manzello SL, Hayashi Y. The size and mass distribution of firebrands collected from ignited building components exposed to wind. Proc Combust Inst 2013;34:2479–85. https://doi.org/10.1016/j.proci.2012.06.061.
[15] Mell W, Maranghides A, McDermott R, Manzello SL. Numerical simulation and experiments of burning douglas fir trees. Combust Flame 2009;156:2023–41. https://doi.org/10.1016/j.combustflame.2009.06.015.
[16] Manzello SL, Cleary TG, Shields JR, Yang JC. Ignition of mulch and grasses by firebrands in wildland-urban interface fires. Int J Wildl Fire 2006;15:427–31.
[17] Wang S, Huang X, Chen H, Liu N. Interaction between flaming and smouldering in hot-particle ignition of forest fuels and effects of moisture and wind. Int J Wildl Fire 2017;26:71–81. https://doi.org/10.1071/WF16096.
[18] Lin S, Zhang T, Huang X, Gollner MJ. The initiation of smouldering peat fire by a glowing firebrand. Int J Wildl Fire 2024;33:1–9. https://doi.org/10.1071/WF23116.
[19] Lin S, Li C, Conkling M, Huang X, Quarles SL, Gollner MJ. Smoldering ignition and transition to flaming in wooden mulch beds exposed to firebrands under wind, Fire Saf. J 2024;148:104226. https://doi.org/10.1016/j.firesaf.2024.104226.
[20] Lauterbach A, Lee S, De Beer J, Stoliarov SI, Sunderland B, Gollner MJ, Filkov AI, Horn GP. Ignition and combustion behavior of pressure treated wood and wood-plastic composite exposed to glowing firebrand piles: impact of air flow velocity,

firebrand coverage density and pile orientation, Fire Saf. J 2024;147:104198. https://doi.org/10.1016/j.firesaf.2024.104198.
[21] Wickramasinghe A, Khan N, Filkov A, Moinuddin K. Physics-based modelling for mapping firebrand flux and heat load on structures in the wildland – urban interface. Int J Wildl Fire 2023:1576–99. https://doi.org/10.1071/WF22119.
[22] Arruda MRT, Cantor P, Bicelli A, Branco F. Thermal reaction of firebrand accumulation in construction materials, Case Stud. Constr Mater 2024;20:e02985. https://doi.org/10.1016/j.cscm.2024.e02985.
[23] Manzello SL, Suzuki S. Influence of board spacing on mitigating wood decking assembly ignition, Fire saf. J 2019;110:102913. https://doi.org/10.1016/j.firesaf.2019.102913.
[24] Fang W, Peng Z, Chen H. Ignition of pine needle fuel bed by the coupled effects of a hot metal particle and thermal radiation. Proc Combust Inst 2021;38:5101–8. https://doi.org/10.1016/j.proci.2020.05.032.
[25] Suzuki S, Manzello SL. Experimental and theoretical approaches to elucidate fuel bed ignition exposed to firebrand showers and radiant heat. Int J Heat Mass Transf 2023;202:123740. https://doi.org/10.1016/j.ijheatmasstransfer.2022.123740.
[26] Suzuki S, Manzello SL. Investigating coupled effect of radiative heat flux and firebrand showers on ignition of fuel beds. Fire Technol 2021;57:683–97. https://doi.org/10.1007/s10694-020-01018-5.
[27] Liu Y, Urban JL, Xu C, Fernandez-pello C. Temperature and motion tracking of metal spark sprays. Fire Technol 2019;55:2143–69. https://doi.org/10.1007/s10694-019-00847-3.
[28] Babrauskas V. Ignition handbook: principles and applications to fire safety engineering, fire investigation, risk management and forensic science. Issaquah: WA: Fire Science Publishers; 2003.
[29] Stokes AD. Fire ignition by copper particles of controlled size. J Electr Electron Eng Aust 1990;10:188–94.
[30] Rowntree GWG, Stokes AD. Fire ignition by aluminium particles of controlled size. J Electr Electron Eng Aust 1994;14:117–23.
[31] Urban JL, Zak CD, Song J, Fernandez-Pello C. Smoldering spot ignition of natural fuels by a hot metal particle. Proc Combust Inst 2017;36:3211–8. https://doi.org/10.1016/j.proci.2016.09.014.
[32] Rein G. Smoldering combustion. SFPE Handb. Fire Prot. Eng. New York, New York, NY: Springer; 2014. p. 581–603. https://doi.org/10.1007/978-1-4939-2565-0_19.
[33] Chen Y, Lin S, Zhang Y, Qin Y, Zhou Y, Wei W, Huang X. Ignition threshold and emission characteristics of self-sustaining smoldering combustion. Combust Flame 2025;281:114411. https://doi.org/10.1016/j.combustflame.2025.114411.
[34] Lin S, Wang S, Huang X. Modeling smoldering ignition by an irradiation spot, Fire saf. J 2022;134:103708. https://doi.org/10.1016/j.firesaf.2022.103708.
[35] Urban JL, Zak CD, Fernandez-Pello C. Spot fire ignition of natural fuels by hot aluminum particles. Fire Technol 2018;54:797–808. https://doi.org/10.1007/s10694-018-0712-4.
[36] Mell WE, Manzello SL, Maranghides A, Butry D, Rehm RG. The wildland-urban interface fire problem - current approaches and research needs. Int J Wildl Fire 2010;19:238–51. https://doi.org/10.1071/WF07131.
[37] Saha S, Ameri E, Avalos J, Cobian-Iñiguez J. Wind-driven ignition behavior of wildland fuels: Experimental insights under controlled conditions. Combust Sci Tech 2026;198:1–18. https://doi.org/10.1080/00102202.2024.2379493.
[38] Wang K, Wang S, Huang X. Hot-particle ignition of typical fuels in the wildland-urban interface and subsequent fire behaviors. Fire Mater 2025;49:698–707. https://doi.org/10.1002/fam.3276.
[39] Viegas DX, Viegas M, Ferreira AD. Moisture content of fine forest fuels and fire occurrence in Central Portugal. Int J Wildl Fire 1992;2:69–86. https://doi.org/10.1071/WF9920069.
[40] Valdivieso JP, Rivera JD. Effect of wind on smoldering combustion limits of moist pine needle beds. Fire Technol 2014;50:1589–605. https://doi.org/10.1007/s10694-013-0357-2.
[41] Ganteaume A, Lampin-Maillet C, Guijarro M, Hernando C, Jappiot M, Fonturbel T, Ṕrez-Gorostiaga P, Vega JA. Spot fires: fuel bed flammability and capability of firebrands to ignite fuel beds. Int J Wildl Fire 2009;18:951–69. https://doi.org/10.1071/WF07111.
[42] Fang W, Yang J, Chen H, Zhang L, Guo P, Yuan Y. Effect of wind velocity on smoldering ignition of moist pine needles by a glowing firebrand. Fire Technol 2024;60:501–17. https://doi.org/10.1007/s10694-023-01520-6.
[43] Rein G. Smoldering combustion. New York, New York, NY: Springer; 2016. https://doi.org/10.1007/978-1-4939-2565-0_19.
[44] Cengel YA, Boles MA. Solutions Manual for Thermodynamics : An Engineering Approach. 8th Edition. SI Units; 2015.
[45] Cengel MABYA. Solutions Manual for thermodynamics : an engineering approach. Solut Man Thermodyn Eng Approach (8th Ed SI Units) 2015.
[46] Ding P, Zhang C, He Q, Wang L, Yang Y. Determining the conditions that lead to the self-extinguished and self-sustained smoldering combustion of wood. Fire 2024;7:1–13. https://doi.org/10.3390/fire7020060.
[47] Wang S, Zhang C, Wang K, Huang X. Ignition limit of EPS foam by a hot particle under cross wind, Case Stud. Therm Eng 2023;51:103523. https://doi.org/10.1016/j.csite.2023.103523.